Inventory of Supplemental Information (*Pillon et al*)

Supplemental data:

- **Figure S1 (most related to Figure 1)**

  Comparison of the C-terminal domains of BsMutL and EcMutL

- **Figure S2 (most related to Figure 3)**

  Structural model for the interaction of BsMutL-CTD and β-clamp

- **Figure S3 (most related to section "A model for the activation of the endonuclease activity")**

  Structural model for the BsMutL-CTD/DNA interaction

- **Movie S1 (most related to section "A model for the activation of the endonuclease activity")**

  Rearrangement of the endonuclease site of BsMutL-CTD in the different crystal forms

Supplemental Experimental Procedures

Supplemental References

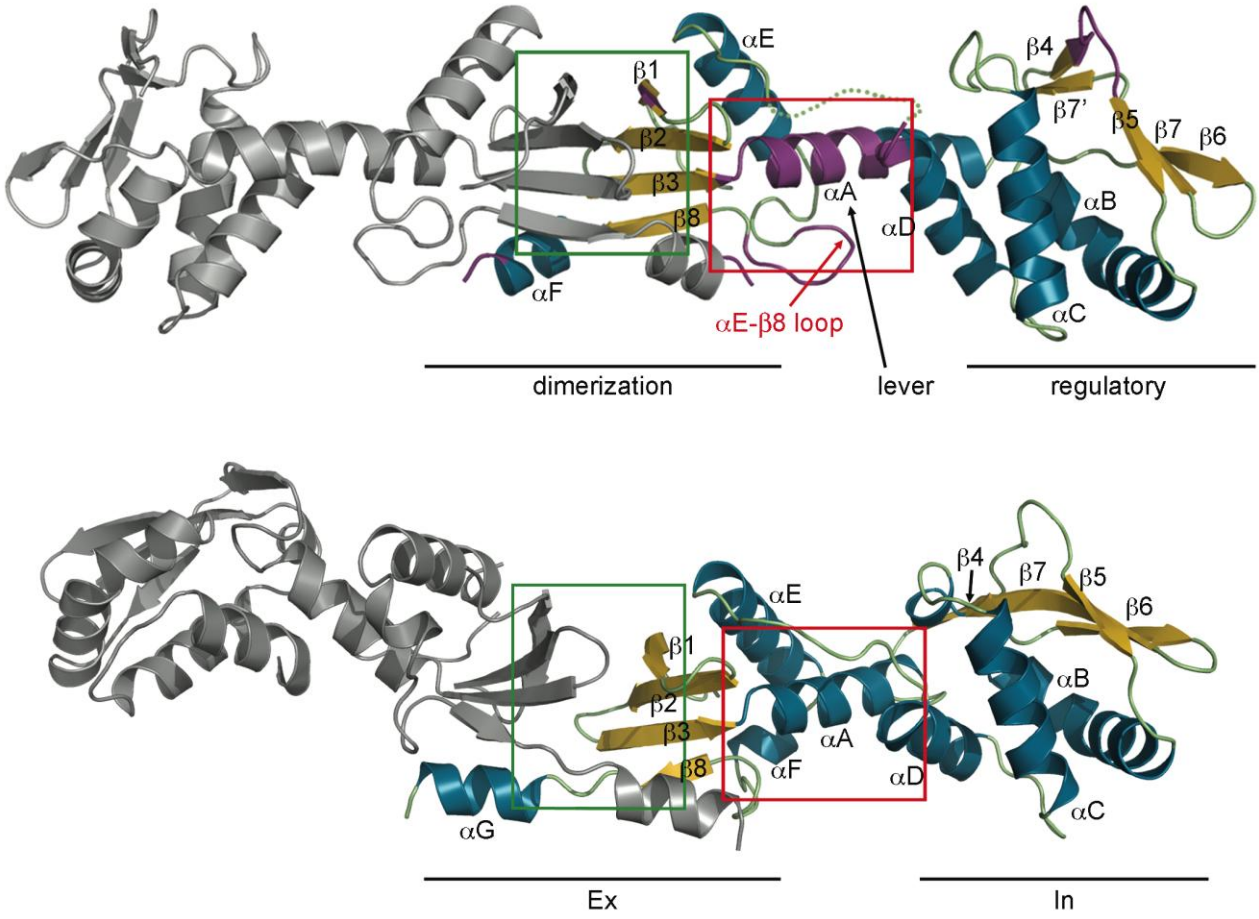

Figure S1 (related to Figure 1): Comparison of the C-terminal domains of *B. subtilis* and *E. coli* MutL. Ribbon diagrams of the BsMutL-CTD (top) and EcMutL-CTD (bottom) dimers. The dimerization and regulatory subdomains, as well as the connecting lever, are labeled. Original names of the EcMutL-CTD subdomains are indicated (Guarné et al., 2004). The most striking differences between the two structures are the dimerization interface (green box) and the organization of the secondary structure elements surrounding helix αA (red box), that would preclude the formation of functional endonuclease site even if EcMutL had the conserved DQHA$(X)_2$E$(X)_4$E, ACR, C(P/N)HGRP and FXR motifs. Note the presence of the extended αE-β8 loop in BsMutL -absent in EcMutL- that secludes the endonuclease site.

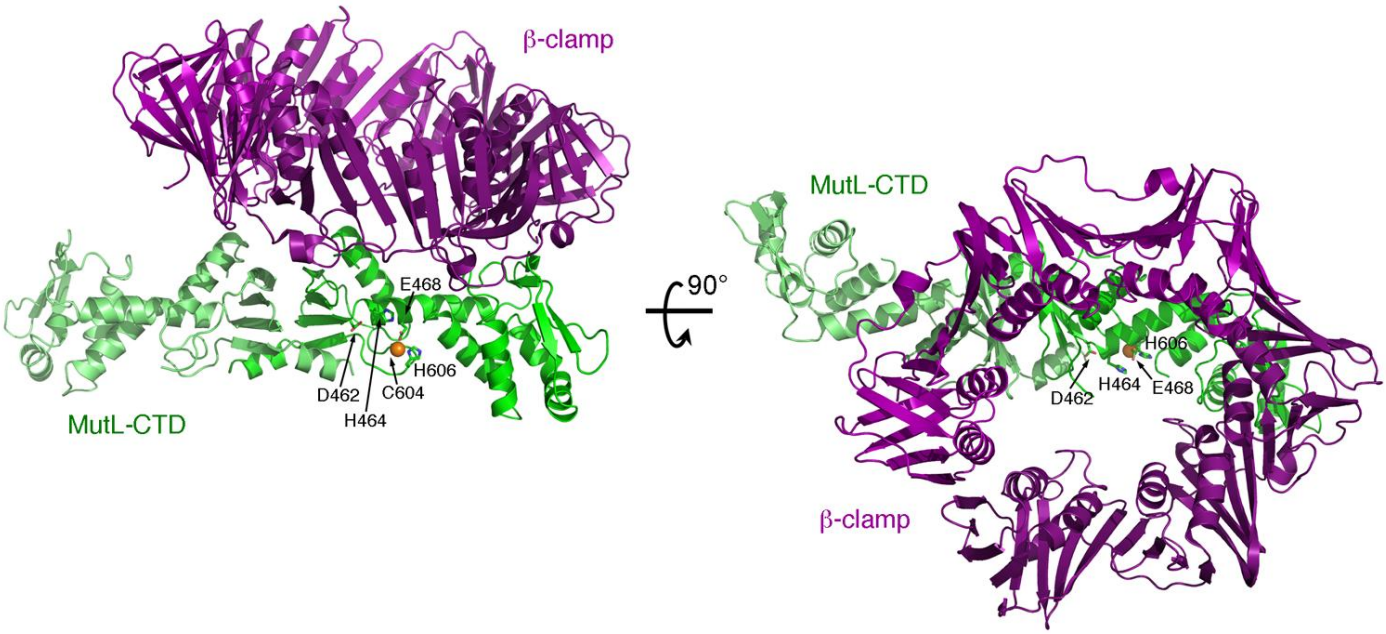

Figure S2 (related to Figure 3): Structural model for the interaction of BsMutL-CTD and β-clamp. Orthogonal views of the structure of the Zn^{2+}-bound form of BsMutL-CTD (crystal form III) shown in green modeled onto the structure of the β-clamp from *E. coli* (purple) in complex with a peptide from polymerase II (PDB ID: 3D1E). To model the complex, residues ^{487}QEMIV for BsMutL-CTD were superimposed onto the polymerase peptide ^{506}QLGLF. The proteins are shown as ribbon diagrams with the side chains involved in catalysis or Zn^{2+}-binding shown as sticks. The Zn^{2+} metal ion is shown as an orange sphere. The model reveals that the interaction of one protomer of the BsMutL dimer with the β-clamp precludes the interaction of the other one due to steric hindrance.

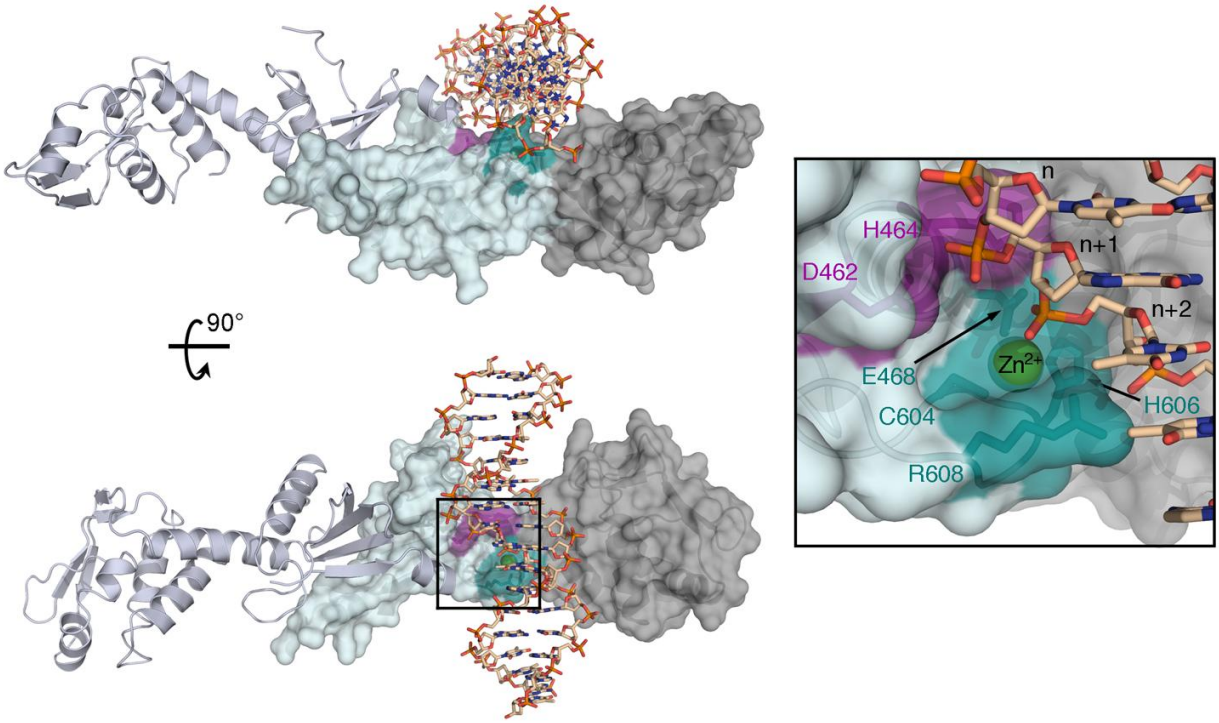

Figure S3 (related to Figure 3): Structural model for the BsMutL-CTD/DNA interaction. A standard B-DNA duplex (PDB ID: 3BSE) was modeled onto the BsMutL-CTD structure (crystal form III) based on four criteria: 1) avoidance of steric hindrance between DNA and protein; 2) distance between Asp462 and the scissile bond compatible with catalysis mediated by one or two metal ions; 3) putative role of the adjacent 3' phosphate group in coordinating the Zn^{2+} metal ion; and 4) electrostatic potential compatibility between the dimerization subdomain and the DNA duplex. The structure of BsMutL-CTD is shown as a ribbon diagram (one protomer) and a surface with the endonuclease site highlighted in purple and the Zn^{2+}-binding site shown in teal (the second protomer). The Zn^{2+} ion is shown as a green sphere and labeled. The DNA structure is shown as color-coded sticks.

Movie S1: Rearrangement of the endonuclease site of BsMutL-CTD in the different crystal forms. Ribbon diagram of the superimposed dimerization subdomains of the four monomers found in crystal form I and the two monomers found in crystal forms II and III. The endonuclease motifs are colored green (^{462}DQHAX$_2$EX$_4$E), purple (^{604}CPHRGP) and orange (^{572}SCK). Hydrogen bonds are shown as black dashed lines and three reference distances (His464 to Glu468, Cys573 to His606 and Glu473 to Ser599) are shown as red dashed lines and labeled. Water molecules are depicted as red spheres and Zn^{2+} ions as lilac spheres.

Supplemental Experimental Procedures

Cloning, purification and crystallization

Full-length BsMutL was amplified from genomic DNA and cloned into the pProEXHTa expression vector (Life Technologies). His-tagged BsMutL was purified using a Ni^{2+}-chelating affinity column equilibrated with 20 mM TRIS pH 8, 0.5 M NaCl, 1.4 mM β-mercaptoethanol, 5% glycerol and 100 mM PMSF. BsMutL was eluted using 300 mM imidazole and subsequently injected on a hydrophobic column equilibrated with 20 mM TRIS pH 8, 1 M KCl, 1 mM DTT and 5% glycerol. BsMutL was further purified by ionic exchange and size exclusion chromatography (MonoQ 5/50 and Superdex-S200, GE Healthcare) equilibrated with 20 mM TRIS pH 8, 100 mM KCl, 1 mM DTT and 5% glycerol (storage buffer). A structure-based sequence alignment was used to subclone the C-terminal fragment of BsMutL (BsMutL-CTD, residues 433-627). BsMutL-CTD was purified similarly to BsMutL with an additional ionic exchange purification step after His-tag cleavage with TEV-protease. Mutants of BsMutL and BsMutL-CTD were generated by QuikChange (Stratagene) and verified by DNA sequencing (MOBIX, McMaster University).

Crystal form I was grown in 25% PEG-monomethyl ether 550, 0.1 M $MgCl_2$, 0.1 M TRIS pH 9 and 5% PEG 400. Two additional crystal forms were obtained when the protein was supplemented with 50 nM $ZnCl_2$ and 50 nM $CoCl_2$. Crystal form II was grown in 25 % PEG 3,350, 0.15-0.2 M NaCl and 0.1 M TRIS pH 7. Addition of 0.1 mM $ZnCl_2$ to this crystallization solution yielded crystal form III. 10 % PEG 400 was added to all crystallization conditions prior to flash freezing in liquid nitrogen.

Data collection and structure determination

For crystal form I, a three-wavelength MAD data set was collected at X29B in NSLS, Brookhaven National Laboratory (Upton, NY). Data were indexed, processed and merged using HKL2000 (Otwinowski and Minor, 1997). Twenty-seven out of thirty-six Selenium sites were found and refined using SOLVE (Terwilliger and Berendzen, 1999). A native data set to 2.5 Å was used for subsequent manual building and refinement, which was done using standard protocols in phenix.refine and COOT (Afonine et al., 2005; Emsley and Cowtan, 2004). Complete data sets of crystal forms II and III, were collected at the X25 beamline in NSLS. Data were collected at a wavelength corresponding to the Zn^{2+}-absorption edge (Table 1), as measured using fluorescence scans. All final models have over 92% of the residues within the most favored regions in the Ramachandran plot and none in disallowed regions. Figures depicting molecular structures were generated using PyMol (DeLano, 2002).

Endonuclease and DNA-binding assays

BsMutL nicking activity was assayed on supercoiled pUC19 (Fermentas). Digestion with the nicking enzyme NbBsrDI (New England Biolabs) was used as a positive control. DNA (5 nM) was incubated with MutL (250 nM, dimer) in 20 mM HEPES pH 7.5, 20 mM KCl, 0.2 mg/mL bovine serum albumin, 1% glycerol (endonuclease buffer) and 5 mM divalent ion for 90 minutes at 37 ˚C. Nicking reactions were stopped with 0.5 mM EDTA and proteinase K (for 15 minutes at 55 ˚C).

To assess DNA binding by BsMutL, supercoiled DNA (5 nM) was incubated with BsMutL variants (100 nM, dimer) in endonuclease buffer for 90 minutes at 37 ˚C. Reaction

mixtures (20 μL) were resolved on 1% TAE agarose gels and quantified using a UVP BioDoc-It™ System and ImageJ (http://rsbweb.nih.gov/ij/).

Zinc-affinity fluorescence assay

Wild type and variants of BsMutL-CTD (2 μM) were incubated with 1 μM FluoZin-3 (Invitrogen) in 10 mM HEPES pH 6 and 200 mM KCl buffer treated with 1% Chelex-100 (Fluka). A calibration fluorescence curve was generated using buffer including increasing concentrations of $ZnCl_2$ (0.25-3 μM) in the absence of protein. Spectra (500-600 nm) were recorded at an excitation wavelength of 494 nm (corrected for buffer effects). Inner-filter effects were neglected because a linear fluorescence intensity response up to stoichiometric amounts of Zn^{2+} was seen when using 4 μM FluoZin-3.

Mismatch repair assays of BsMutL variants

Relative mutation frequency was determined as described earlier (Simmons et al., 2008). *B. subtilis* cells were grown at 37 ^{o}C to $O.D._{600}$ of ~1.0, collected by centrifugation and resuspended in 0.85% saline. A portion of the cells was serial diluted into 0.85% saline followed by plating on LB agar for determining the number of viable cells per mL of culture. The remaining portion of cells was plated on LB agar plates supplemented with 100 μg/mL rifampicin. The mutation frequency was determined for each strain by comparing the number of rifampicin resistant cells relative to the number of viable cells. The mutation frequency was then normalized to the mutation frequency obtained for the wild type control strain LAS284 (relevant genotype: *amyE*::P_{spank}*mutL*$^{+}$, *mutL*::*spc*) (see table below). LAS284 was used because each *mutL* variant was expressed in single copy from the *amyE* locus under control of the P_{spank} IPTG

inducible promoter. The native *mutL* gene was inactivated by insertion of a spectinomycin resistance cassette (Simmons et al., 2008). The mutation frequency of LAS284 is 1.8-fold higher than the parent strain PY79. The observed mutation frequency for wild type PY79 is $2.77X10^{-9} \pm 9.10X10^{-10}$.

List of *B. subtilis* strains

Strain	Relevant Genotype	Reference
PY79	Prototroph, SPβ^{o}	(Youngman et al., 1984)
LAS284	*amyE*::P$_{spank}$*mutL*$^{+}$, *mutL*::*spc*	This work
AK31	*amyE*::P$_{spank}$*mutL (D462A), mutL*::*spc*	This work
AK32	*amyE*::P$_{spank}$*mutL (Q463A), mutL*::*spc*	This work
AK33	*amyE*::P$_{spank}$*mutL (H464A), mutL*::*spc*	This work
AK34	*amyE*::P$_{spank}$*mutL (Q487A), mutL*::*spc*	This work
AK35	*amyE*::P$_{spank}$*mutL (I490D), mutL*::*spc*	This work
AK36	*amyE*::P$_{spank}$*mutL (P492A), mutL*::*spc*	This work
AK37	*amyE*::P$_{spank}$*mutL (H606A), mutL*::*spc*	This work
AK38	*amyE*::P$_{spank}$*mutL* (^{487}*AAAAA*^{491}), *mutL*::*spc*	This work
LAS286	*amyE*::P$_{spank}$*mutL (E468K), mutL*::*spc*	This work
LAS287	*amyE*::P$_{spank}$*mutL (E473K), mutL*::*spc*	This work

Supplemental References

Afonine, P.V., Grosse-Kunstleve, R.W., and Adams, P.D. (2005). phenix.refine. CCP4 Newsletter *42*, contribution 8.

DeLano, W.L. (2002). The PyMOL Molecular Graphic Systems (Palo Alto, CA, USA: DeLano Scientific).

Emsley, P., and Cowtan, K. (2004). Coot: model-building tools for molecular graphics. Acta Crystallogr D Biol Crystallogr *60*, 2126-2132.

Otwinowski, Z., and Minor, W. (1997). Processing of X-ray Diffraction Data Collected in Oscillation Mode. In Methods in Enzymology, C.W. Carter, and R.M. Sweeet, eds. (New York: Academic Press), pp. 307-326.

Simmons, L.A., Davies, B.W., Grossman, A.D., and Walker, G.C. (2008). Beta clamp directs localization of mismatch repair in Bacillus subtilis. Mol Cell *29*, 291-301.

Terwilliger, T.C., and Berendzen, J. (1999). Automated structure solution for MIR and MAD. Acta Crystallo. D *55*, 849-861.

Youngman, P., Perkins, J.B., and Losick, R. (1984). Construction of a cloning site near one end of Tn917 into which foreign DNA may be inserted without affecting transposition in Bacillus subtilis or expression of the transposon-borne erm gene. Plasmid *12*, 1-9.